Computer Assisted Methods in Engineering and Science
32(2): 213–234, 2025, https://doi.org/10.24423/cames.2025.1805

Damage Localization Using Fiber Bragg Grating Sensors in Self-referencing Configuration: A Numerical Study

Abhishek PATANGE[1)], Farzam Omidi MOAF[2),3)], Piotr FIBOREK[2)], Adityan ARUMUGANAINAR[4)], Rohan SOMAN[2)*]

[1)] *School of Mechanical Engineering, Vellore Institute of Technology, Chennai, India*

[2)] *Institute of Fluid Flow Machinery, Polish Academy of Sciences, Gdańsk, Poland*

[3)] *Faculty of Civil and Environmental Engineering, Gdańsk University of Technology, Gdańsk, Poland*

[4)] *COEP Technological University, Shivajinagar, Pune, Maharashtra, India*

[*] *Corresponding Author e-mail: rsoman@imp.gda.pl*

This study investigates a self-referencing method for damage detection and localization using guided waves (GW) sensed by fiber Bragg grating (FBG) sensors. The research integrates advanced numerical simulations with an innovative configuration of sensors to enhance structural health monitoring (SHM). A self-referencing setup, employing FBG sensors with edge filtering method and remote bonding, enables a baseline-free damage detection approach. The methodology is validated as a proof-of-concept numerical model. The simulation framework incorporates a three-dimensional spectral element method for precise and efficient modelling of GW propagation and interactions with structural anomalies. Three different machine learning (ML) techniques are employed to detect and localize damages, demonstrating effectiveness of ML methods compared to traditional methods.

The three techniques employed are decision tree, logistic model tree and random forest. Key findings highlight the effectiveness of random forest models in classifying damage states with a 98.67% accuracy. Different feature selection methods, are used to identify critical features. The proposed methodology reduces sensor requirements, lowers system complexity and cost, and enables efficient SHM solutions in extreme or large-scale environments. This work underscores the potential of ML techniques to perform detection and localization where traditional techniques fail.

Keywords: guided waves (GW), fiber Bragg grating (FBG) sensors, damage detection, self-referencing method, machine learning (ML) referencing method, numerical simulation.

Copyright © 2025 The Author(s).
Published by IPPT PAN. This work is licensed under the Creative Commons Attribution License CC BY 4.0 (https://creativecommons.org/licenses/by/4.0/).

1. Introduction

Structural health monitoring (SHM) has garnered significant research interest over the past few decades due to its substantial economic benefits. Beyond cost savings, SHM techniques enhance structural safety and reliability, and in some cases, can extend the structure lifespan. Numerous techniques have been developed to monitor a variety of damage-sensitive features, including vibration [1], strain [2], wave propagation [3], and electromagnetic impedance [4] signatures. Each technique presents distinct advantages and limitations, necessitating careful selection of the most suitable approach based on application-specific requirements, such as damage tolerance and degradation mechanisms. Among SHM methods, guided wave (GW)-based techniques are particularly effective for monitoring thin-walled structures. GW can propagate over large distances with minimal attenuation, enabling the inspection of large areas with a limited number of sensors. Additionally, their short wavelengths associated with GW enhance their sensitivity to minor damage, which is especially valuable in structures with low damage tolerance. GW-based techniques have been developed for damage detection and localization in structures. Most commonly used damage sensitive features include amplitude changes along the wave propagation path [5], time of arrival (ToA) of reflected/scattered signals followed by triangulation [6], and non-linear signatures due to damage [7]. More recently, the artificial intelligence (AI)-based technique have also emerged [8,9]. An excellent overview of different damage detection and localization techniques can be found in [3,10–12].

Several sensor systems have been developed for GW detection, including piezoelectric (PZT) sensors, macro fiber composites (MFC), optical fiber sensors, and non-contact methods such as laser Doppler vibrometers [13]. The use of optical fiber sensors for GW sensing is attracting renewed interest within the SHM community. Optical fiber sensors utilizing fiber Bragg gratings (FBG) present several distinct advantages, such as compact size, low weight, embeddability, and multiplexing capabilities. These attributes make FBG sensors highly suitable for a wide array of applications, including civil engineering [14], wind energy [15], marine structures [16], and aerospace engineering [17]. Traditionally, FBG sensors are employed in a wavelength division multiplexing (WDM) configuration, where changes in wavelength are detected and calibrated to measure strain or temperature. However, this approach is limited to static or quasi-static conditions and lacks the sensitivity required for high sampling rate applications, such as GW sensing. To address this limitation, edge filtering technique has been utilized. This approach enhances the sensitivity and effectiveness of FBG sensors in dynamic GW monitoring context. In the edge filtering approach, a tunable laser is aligned on either the upward or downward slope of the FBG spectrum.

Spectral shifts in the FBG induce changes in reflectivity, which can be detected as amplitude variations through a photodetector. The high slope of the FBG enhances sensitivity by amplifying spectral changes, and commercially available high-speed photodetectors (with sampling rates in GHz) make this approach feasible for dynamic applications [18].

Beyond the exceeding inherent benefits, FBG sensors offer additional unique advantages for GW sensing. One such feature is remote configuration, where the optical fiber serves as a mechanical waveguide, capable of transmitting mechanical waves over several meters with minimal attenuation [19]. This property can be strategically utilized for sensor deployment in extreme environments [20], while simultaneously reducing equipment costs by enabling multi-point measurements with a single sensor system [21]. Another innovative arrangement is the self-referencing configuration that further expands the versatility of FBG-based GW sensing for SHM applications [22].

FBG sensors in the remote configuration with the edge filtering approach offer enhanced sensitivity and can also be implemented in a self-referencing setup (Fig. 1). In this configuration, a wave is generated at a PZT and travels along the structure until it reaches Bond 1, where it couples with the optical fiber and is transmitted to the FBG for sensing. This initial wave packet contains information about the undamaged structure. The wave then continues propagating through the structure, interacting with any damage, before reaching Bond 2. At this point, the wave – now influenced by structural damage – couples to the optical fiber and is sensed by the FBG.

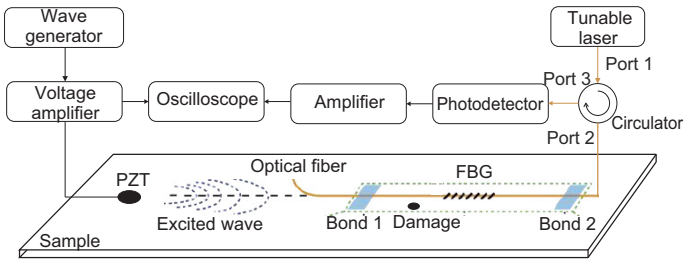

FIG. 1. Schematic explaining self-referencing configuration (based on [22]).

The difference in information encoded within the two wave packets, captured at Bond 1 and Bond 2, can be utilized for damage detection and localization, even in the absence of baseline measurement from the undamaged structure. This capability for reference-free damage detection is particularly advantageous for SHM applications in aging infrastructure, as it simplifies implementation and broadens the applicability of SHM techniques [23]. The novel integration of self-referencing configuration with edge-filtered FBG sensors introduces a new level of sensitivity and reliability for GW sensing in SHM. By eliminating the need for

baseline measurement, this approach offers a streamlined and adaptable solution for monitoring aging infrastructure, particularly in extreme and large-scale environments. Furthermore, this configuration enables multi-point measurements with fewer sensors, substantially reducing system complexity and cost. These contributions mark a significant advancement in SHM technology, demonstrating both practical and theoretical advancements that open new possibilities for structural health management across various engineering fields. The effectiveness of the configuration for detecting damage was studied by Wee *et al.* [22]. But their implementation still relied on measurement of a baseline. The present work aims to utilize the self-referencing configuration of FBG sensors to develop a reference-free damage detection and localization technique, representing the main novelty of this research. The methodology is investigated through a validated numerical model as a proof-of-concept.

The rest of the paper is organized as follows: Sec. 2 explains the numerical setup. Section 3 shows the limitations of the traditional technique based on time of arrival (ToA). As a result a data-driven ML-based technique is utilized for damage detection and localization. Section 4 outlines the methodology applied, including the methods used for feature selection. The training and testing results along with discussions are presented in Sec. 5. Finally, based on the presented results, conclusions are drawn in Sec. 6. Section 6 also identifies areas of further research.

2. Numerical setup

Simulating GW propagation in structures is inherently challenging due to varying temporal and spatial scales involved. For example, the time increment needed for accurate GW simulation is in the order of nanoseconds, while the total simulation duration spans hundreds of microseconds, requiring thousands of time steps. In the spatial domain, the optical fiber under consideration with a diameter of 125 μm demands numerous nodes across each cross-section for accurate modeling. Additionally, both plate and fiber lengths are of the order of meters. As a result, the number of elements and associated computational load is quite large. Traditional finite element (FE) methods prove insufficient for handling these diverse scales efficiently. To address this, we implemented a time-domain spectral analysis method (SEM) with non-matching interface elements that establish connections between the adhesive layer and host plate. The SEM uses high-order Lagrange polynomial interpolation to define shape functions within spectral elements. Furthermore, a Gauss–Lobatto–Legendre integration scheme was employed for the necessary numerical integration. This approach is essential for analyzing GW propagation characteristics and their interactions with potential structural anomalies. The strategy for the non-matching grids

has been explained by Fiborek *et al.* [24]. This approach significantly reduces computational costs by lowering the number of elements while maintaining the accuracy needed for analyzing GW propagation. The numerical modeling has been explained in detail and experimentally validated in [24].

An aluminum plate (Fig. 2a) with dimensions 1000 mm × 500 mm × 1 mm was modeled. The self-referencing configuration was implemented as shown in Fig. 2a. The modeling strategy for the optical fiber and adhesive bond is shown in Fig. 2b. Damage was simulated at different locations along the line connecting the two bonds as a through-thickness hole of 8 mm diameter. The authors acknowledge that an 8 mm diameter represent significant damage, this obvious damage scenario was selected to serve as a clear proof-of-concept demonstration for the self-referencing approach. The simulation utilized a three-dimensional spectral element method, comprising a total of 2 106 428 nodes.

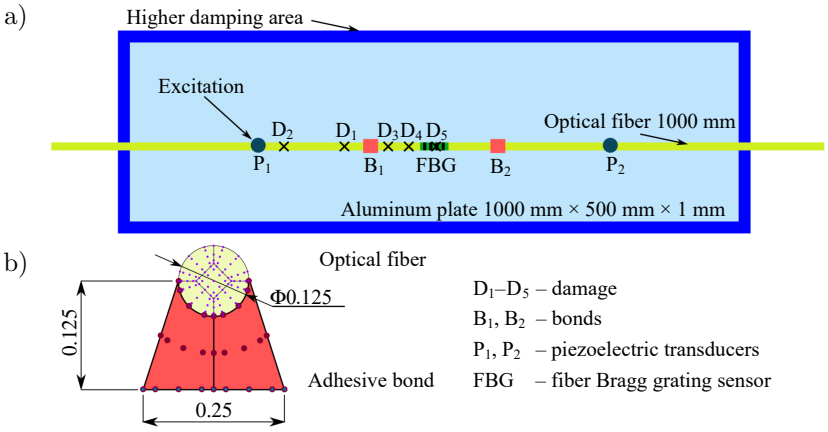

FIG. 2. Structural model (a) top view of the sample, (b) cross-section of the optical fiber and adhesive bond.

The excitation of the GW was achieved through the application of a 5.5-cycle Hann-windowed sine wave, characterized by a frequency of 300 kHz. The excitation signal was chosen similar to the approach of Wee *et al.* [22] who proposed the self-referencing configuration. The time period of this signal was set at 200 μs, with a time increment of 3.8×10^{-10} s. Strain and displacements at the core of the optical fiber locations where the FBG was located were then extracted and converted to the FBG response using the transformation matrix from Wee *et al.* [25]. The time signal for one of the cases is shown in Fig. 3. The first packet (n_1) that arrived at the FBG sensor is the packet of L_{01} mode converted from the S_0 mode at Bond B_1, while the second one (n_2) is a superposition of the mode L_0 converted from the S_0 mode at Bond B_2 and the packet n_1 reflected from B_2. Due to the similar group velocity of the S_0 mode in the host plate and packet n_1 in the optical fiber, n_2 results in an amplification of the two packets.

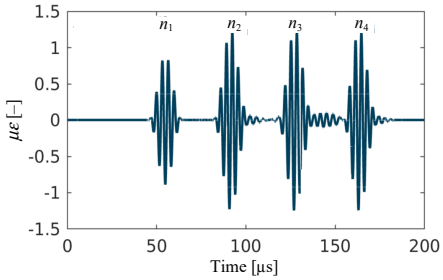

FIG. 3. Simulated time signal for healthy condition.

Then, packet n_3 is the reflection of n_2 from B_1, and finally, packet n_4 is the reflection of n_3 from B_2.

The FBG response was then contaminated with 10% white noise, and 50 such repetitions were generated to simulate 50 different measurements. These datasets were used for both traditional method and the ML algorithm. It should be noted that this data augmentation approach using white noise is a commonly used strategy for improving classifier performance [26].

3. Analytical methodology

The traditional damage localization method relies on baseline subtraction and identifying the ToA of the wave packet generated due to damage. In order to effectively identify the effect of damage, baseline subtraction needs to be performed. As the aim of this paper is to develop a reference-free technique, the baseline signal was constructed analytically. For this construction of analytical baseline signal, the physics of the system was considered: the wave coupled at Bond 1 is detected as the first wave packet. The second wave packet is a combination of the reflection of the first wave in the fiber and the wave coupled at Bond 2. In the absence of material damping and assuming perfect coupling of the fiber at the bond location, the amplitude of the second wave packet would be twice that of the first packet. But, in reality, due to material damping in both the plate and the fiber, as well as imperfect coupling at the bonds, the magnitude of the second peak is lower than twice that of the first. Empirically (from a simulated healthy structure) this ratio was determined as 1.38 times that of the first wave packet. Based on the first wave packet amplitude and ToA (Fig. 4a), the analytical healthy signal was constructed by shifting the envelope by a number of time steps corresponding to the distance between the two bonds and the velocity of the L_{01} wave in the fiber, the multiplying by the factor 1.38 (determined empirically). This analytical signal (Fig. 4b) was then used for baseline subtraction. The envelope of the measured signal (Fig. 4c) was then subtracted from the analytical signal to obtain the residual (Fig. 4d), which was used to identify

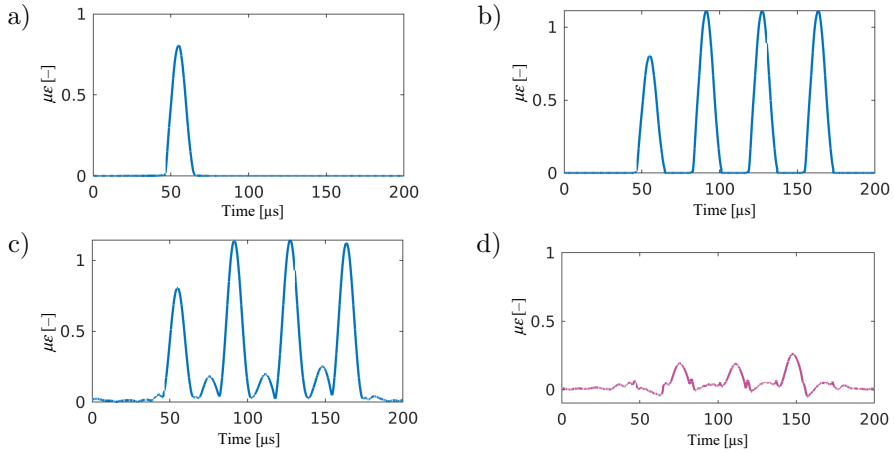

FIG. 4. Methodology for ToA-based damage localization: a) first package, b) analytical baseline signal (amped up & duplicated), c) measured signal, d) residual signal (subtraction).

peaks associated with wave packet due to the scattering effect of damage. In order to determine this, a threshold value of 15% was chosen. This value was chosen to account for 10% noise in the time signals. To summarize, the following steps were necessary for damage localization:

1. Obtain the analytical baseline signal using first package arrival information and subsequent wave packets.
2. Obtain the residual by subtracting the measured signal from the analytical baseline.
3. Identify peaks in the residual signal above the threshold.
4. Locate damage based on the propagation velocity and ToA.

Once the peak exceeding the determined threshold was identified, the location of the damage could be detected based on Eq. (3.1). The ToA is a well-known metric used for damage detection and localization [6, 27],

$$d = c_g \frac{\Delta t}{2}, \tag{1}$$

where c_g is the group velocity of the S_0 wave, and Δt is the time difference between signals.

Baseline subtraction was applied to different simulated damage scenarios. For brevity, the residuals (after baseline subtraction) are shown for four cases in Fig. 5. In the pristine case, where no damage is present, none of the peaks exceed the threshold, serving as confirmation of correct level 1 damage detection. In case damage 5, the threshold is not exceeded, resulting in a false positive result, i.e., the structure is falsely identified as healthy when indeed there is damage. For the other damage cases, the damage was successfully detected and localized.

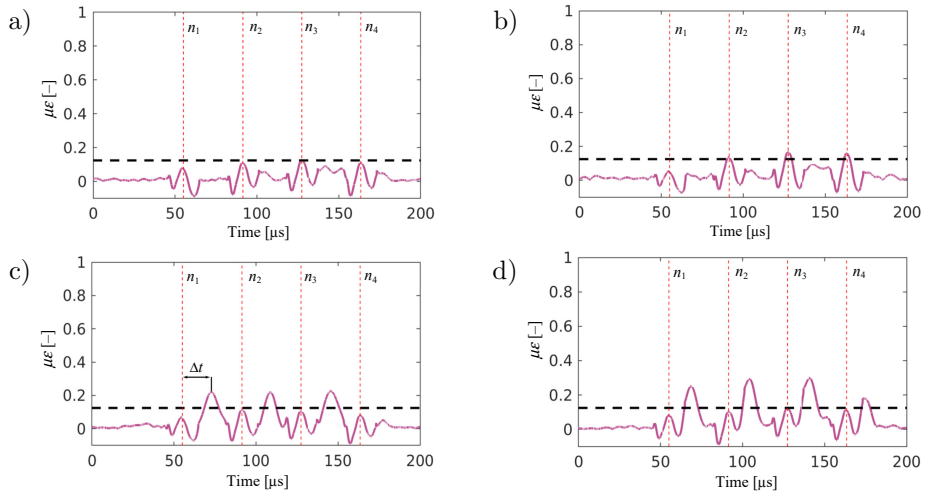

FIG. 5. Residual signal after baseline subtraction: a) healthy, b) case D5, c) case D3, d) case D4.

As shown the conventional method may lead to false detection; furthermore, accurate localization requires knowledge of the exact velocity of propagation in the structure, which in complex anisotropic structures is a challenge. Lastly, the extraction of the exact ToA of the waves continues to remain a challenge due to the multi-modal nature of the excited GWs and their complex interactions with structural components. In order to overcome these challenges, ML-based algorithms were investigated. Applications of ML algorithms in SHM are becoming increasingly common. ML models can extract relevant features from noisy data, model complex non-linear relationships between signals and damage, and adapt to variations in material properties or environmental conditions. Unlike the rigid traditional approach, ML can generalize across diverse scenarios, significantly reducing localization errors and improving accuracy. Furthermore, ML systems can process large datasets in real time, making them scalable and suitable for complex structures [28]. By overcoming the shortcomings of the traditional method, ML provides a powerful and reliable tool for precise damage localization [29].

4. Methodology

There are several different ML techniques that might be employed, including supervised learning, unsupervised learning approaches as well as deep learning techniques. Each of these techniques has its pros and cons. In the current application, we have a relatively small amount of labeled training data. Also, the physics of wave propagation is not completely understood. So, a supervised learning approach was employed. Three different classifiers were implemented to

evaluate their effectiveness in classify different damage cases: decision tree, logistic model tree, and random forest classifier.

A key task in supervised learning algorithms is the selection of appropriate features for training and classification. In order to determine the most suitable set, different feature selection strategies were compared. The input data consisted of time signals for the same case from the two piezoelectric excitations. For each damage class, 50 repetitions were used. Both k-fold classification as well as blind testing with 25% of the data randomly selected was carried out.

4.1. Feature selection

In ML processes, particularly in SHM, it comes in handy to eliminate high-dimensional data points from the dataset, thereby necessitating for feature selection. The use of appropriate feature selection techniques not only improves computation time, and reduces the chances of over-fitting, it also brings forth the most important features that relate to a particular classification. A total of 32 features were investigated. These features are quite standard in ML, and are listed in Fig. 8. In this study, the following methods were used for feature selection:

1. **Variance thresholding**: Features having minimal variance were classified as having no information and excluded from the analysis. This approach enabled to find and remove any features with a variance below 0.01. Figure 6 shows the reduction in features achieved using this method.
    - **Pros**: Simple and computationally efficient; removes low-variance, non-informative features.
    - **Cons**: Ignores feature-target relationships, may potentially discard predictive features.

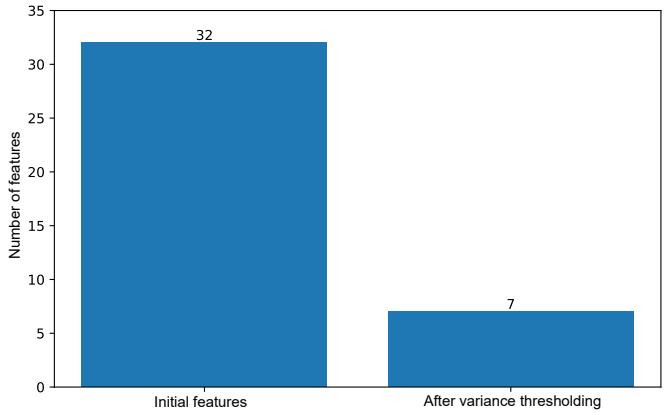

FIG. 6. Number of features before and after variance thresholding.

2. **Univariate selection (ANOVA F-test)**: The importance of specific features in relation to the target feature was estimated using statistical tests. Among F-score variables, Fig. 7 shows these as the 10 best performing variables.
    - **Pros**: Identifies statistically relevant features; easy to interpret and implement.
    - **Cons**: Assumes linear relationships and ignores feature interactions.

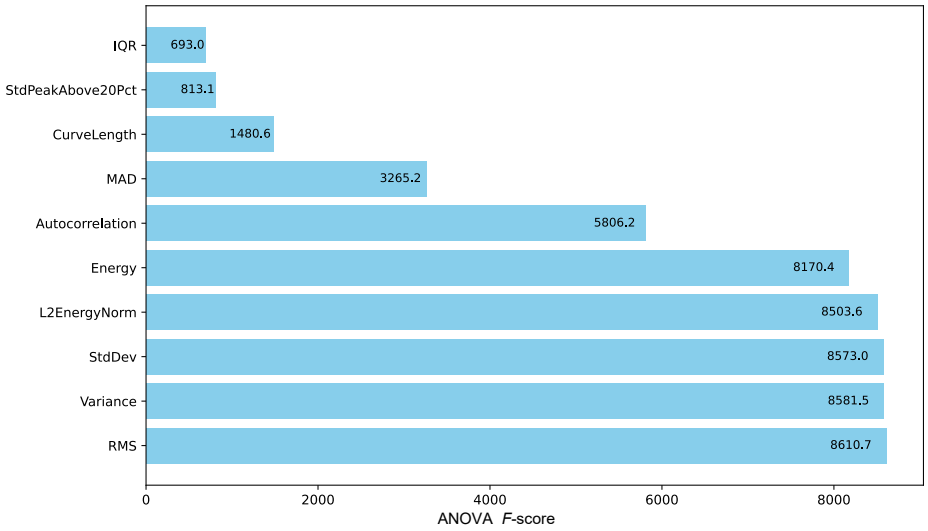

FIG. 7. Top 10 features selected using univariate selection.

3. **Recursive feature elimination (RFE)**: This iterative technique enables a random forest classifier to make predictions, and features are ranked according to their level of importance in further predictions. RFE gave the following ranks, as shown in Fig. 8. The lower rank signifies higher importance of the feature for classification.
    - **Pros**: Considers feature interactions and iteratively selects the most relevant features.
    - **Cons**: Computationally expensive and heavily dependent on the base model's assumptions.
4. **Dimensionality reduction**: To tackle issues of class separability and to visualize the high-dimensional feature space, two notable techniques of dimensionality reduction were employed:
    (a) **Principal component analysis (PCA)**: PCA reduces the dimensionality of the dataset by projecting it into subspaces of lower dimensions while preserving the greatest variance along orthogonal directions in the subspace. The 2D projection obtained from PCA is shown in Fig. 9.

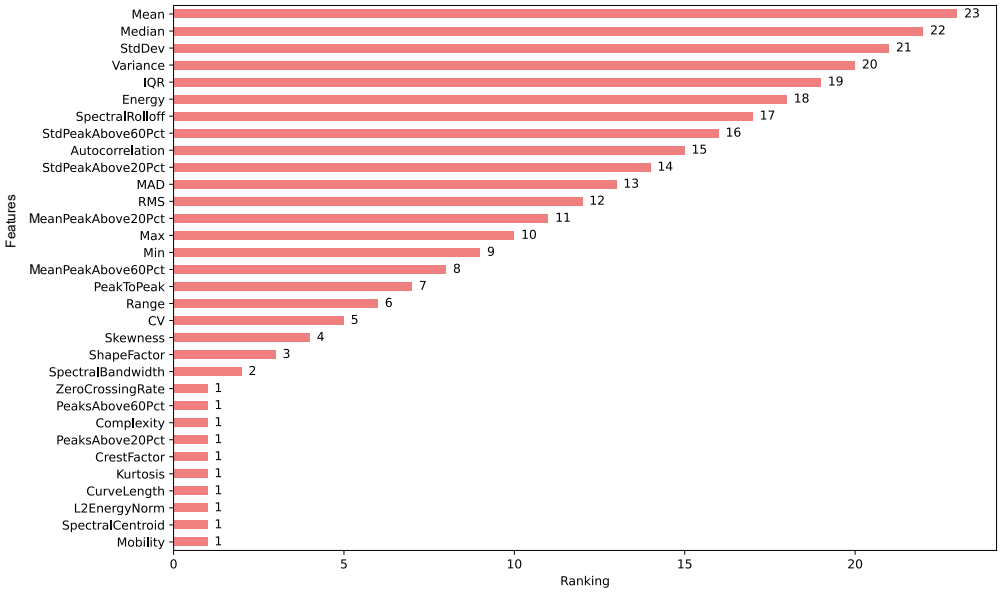

FIG. 8. Feature rankings using RFE.

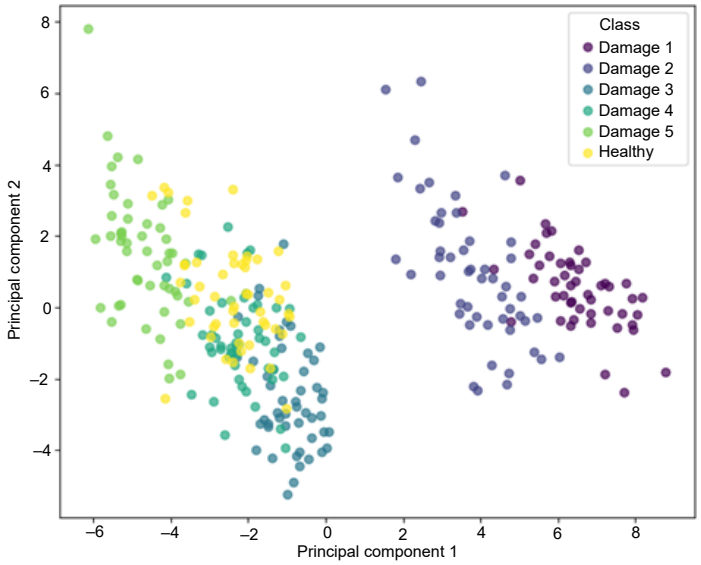

FIG. 9. 2D projection of data using PCA.

(b) **A *t*-distributed stochastic neighbor embedding (*t*-SNE) approach**: *t*-SNE maps the entire dataset into a two-dimensional space while attempting to preserve the topology of the dataset so as to focus on local space. The results of *t*-SNE are highlighted in Fig. 10.

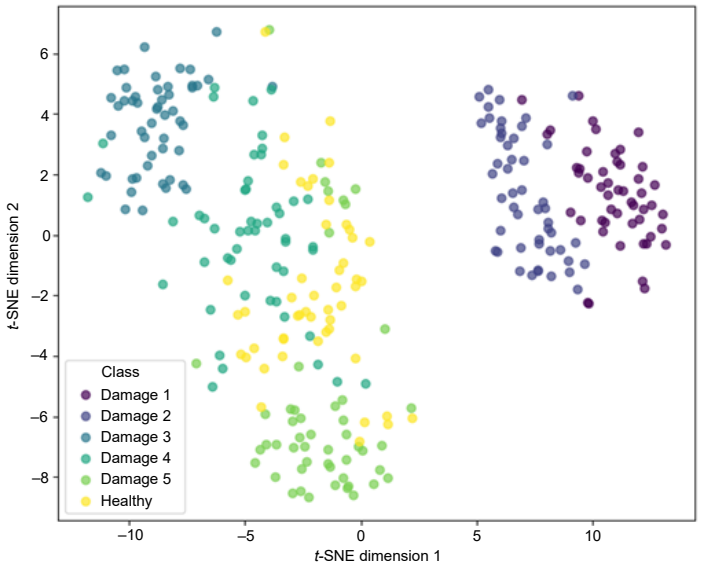

FIG. 10. 2D projection of data using t-SNE.

5. **Tree-based selection**: The 10 most important features were identified using a random forest model. They are displayed in Fig. 11.
   - **Pros**: Captures feature interactions and non-linear relationships; interpretable due to feature importance scores.
   - **Cons**: May introduce bias toward features with high variability or more levels.

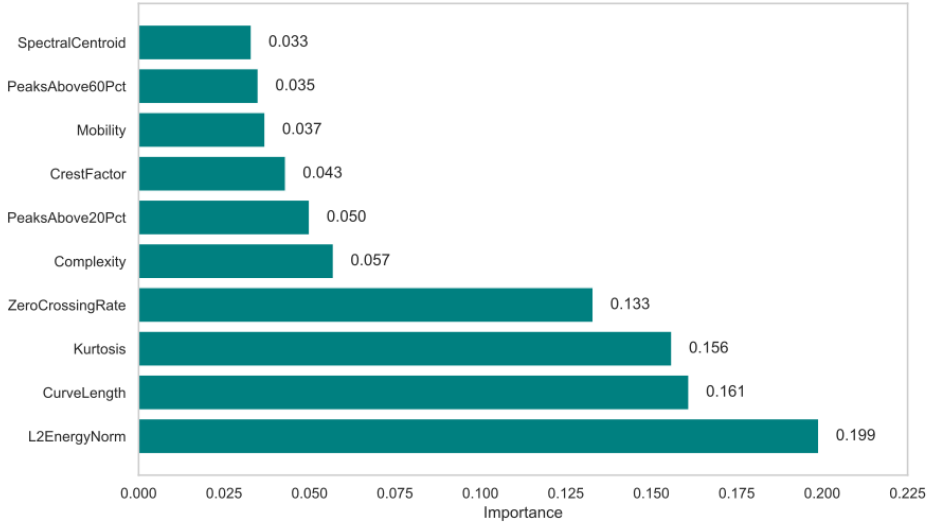

FIG. 11. Top 10 features selected using tree-based feature importance.

In this particular case, tree-based feature selection proved to be the most useful because it models **non-linear relationships** and accounts to **feature interactions** which is essential for distinguishing of damage states in SHM datasets. Its **interpretability** in terms of feature importance scores facilitated validation by relevant domain experts. This level of interpretability is absent in other methods, for example in variance thresholding or ANOVA, which makes tree-based selection as the most effective as tradeoff between performance and complexity.

5. Results

The most informative features were identified. These features were then utilized with three different techniques (namely, decision tree, logistic model tree and random forest) for k-fold cross-validation as well as testing on unseen data. It should be noted that the k-fold validation uses all the data for the cross-validation ($k = 10$). The aim of cross-validation was to reliably estimate model performance, and to reduce bias, if any, in the training data. For testing, the models were retrained, separately with a 75/25 split, where 75% of the data was randomly chosen and utilized for training, and the remaining 25% data was unseen by the models and used for testing. The results of both cross-validation and testing were compared using evaluation metrics such as true positive (TP) rate, false positive (FP) rate, precision, recall, and the confusion matrix.

5.1. Decision tree

Using the decision tree on a dataset of 300 cases (50 repetitions each for 5 damage classes, and 50 repetitions for the class healthy), 256 (85.33%) were correctly classified, while 44 (14.67%) were incorrectly classified. The class-wise accuracy table and confusion matrix are shown in Table 1 and Fig. 12, respectively.

Table 1. Class-wise accuracy table.

Class	TP rate	FP rate	Precision	Recall
Healthy	0.80	0.052	0.755	0.80
Damage 1	0.78	0.016	0.907	0.78
Damage 2	0.90	0.044	0.804	0.90
Damage 3	1.00	0.000	1.000	1.00
Damage 4	0.88	0.002	0.898	0.88
Damage 5	0.76	0.044	0.776	0.76

For testing, 75 random time signals were chosen; the confusion matrix and accuracy table for this testing are given in Fig. 13 and Table 2, respectively.

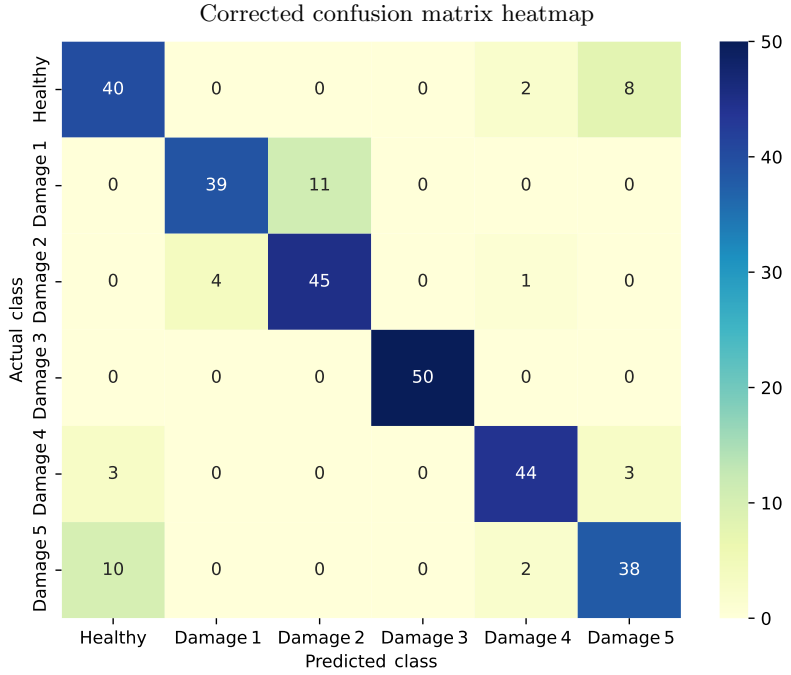

FIG. 12. Cross-validation results for decision tree.

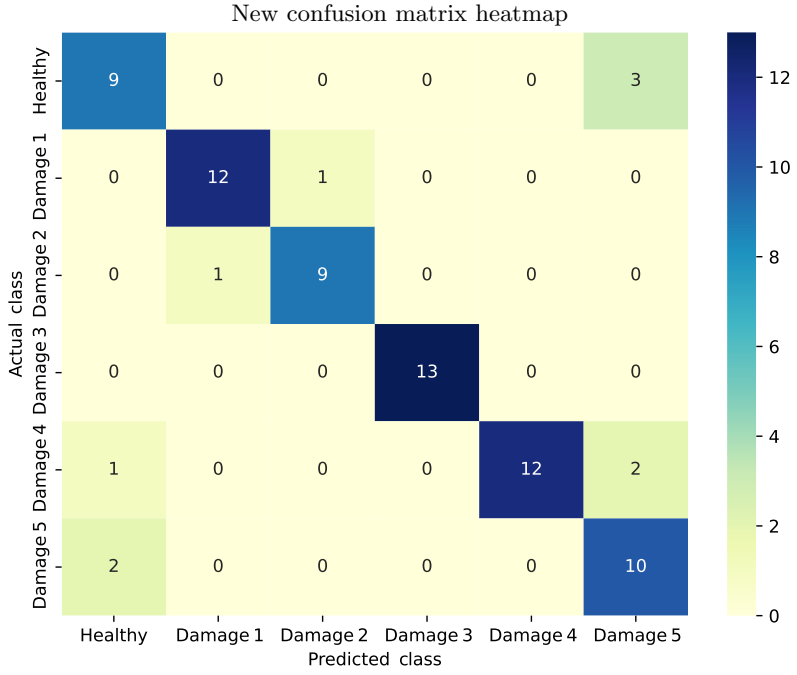

FIG. 13. Test results for decision tree.

TABLE 2. Class-wise accuracy table.

Class	TP rate	FP rate	Precision	Recall
Healthy	0.750	0.048	0.750	0.750
Damage 1	0.923	0.016	0.923	0.923
Damage 2	0.900	0.015	0.900	0.900
Damage 3	1.000	0.000	1.000	1.000
Damage 4	0.800	0.000	1.000	0.800
Damage 5	0.833	0.079	0.667	0.833

It can be seen that the accuracy does not change appreciably between cross-validation and testing scenarios.

5.2. Logistic model tree

The logistic model tree (LMT) showed a higher accuracy (94.33%) in cross-validation compared to the decision tree. Figure 14 and Table 3 show the confusion matrix and class-wise accuracy, respectively.

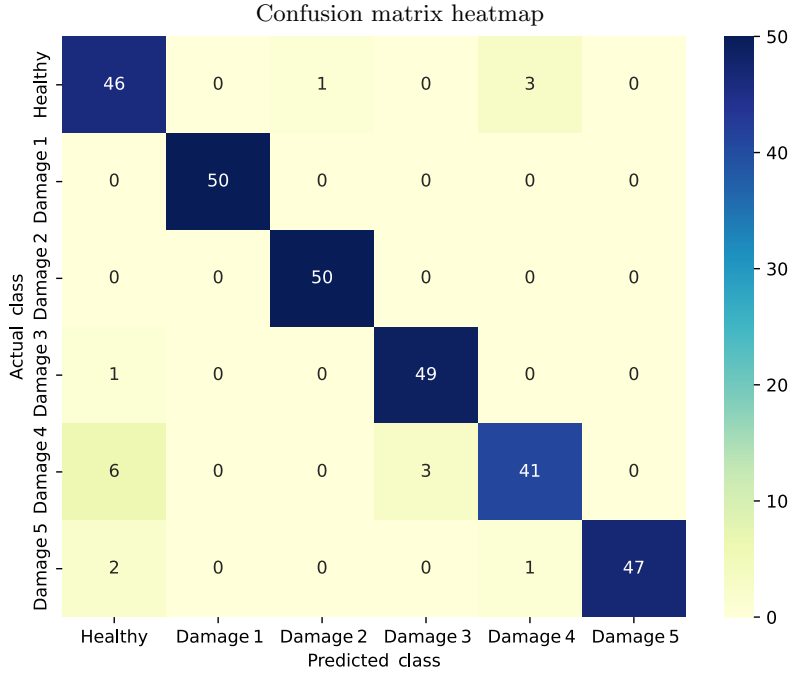

FIG. 14. Cross-validation results for LMT.

The performance of the logistic model tree on the testing dataset is shown in Fig. 15 and Table 4. The model achieved an accuracy of 96% during testing.

Table 3. Class-wise accuracy table.

Class	TP rate	FP rate	Precision	Recall
Healthy	0.920	0.036	0.836	0.920
Damage 1	1.000	0.000	1.000	1.000
Damage 2	1.000	0.004	0.980	1.000
Damage 3	0.980	0.012	0.942	0.980
Damage 4	0.820	0.016	0.911	0.820
Damage 5	0.940	0.000	1.000	0.940

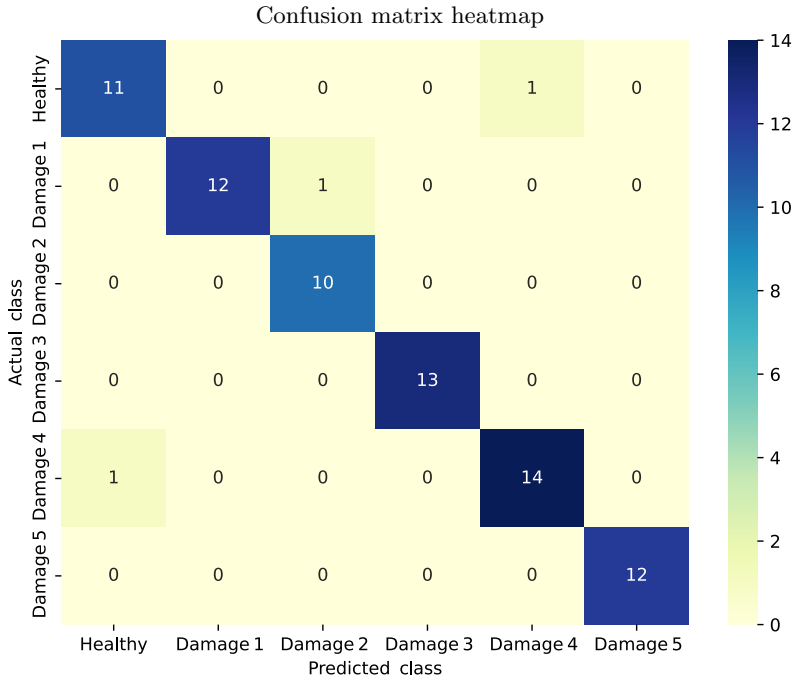

Fig. 15. Test results for LMT.

Table 4. Class-wise accuracy table.

Class	TP rate	FP rate	Precision	Recall
Healthy	0.917	0.016	0.917	0.917
Damage 1	0.923	0.000	1.000	0.923
Damage 2	1.000	0.015	0.909	1.000
Damage 3	1.000	0.000	1.000	1.000
Damage 4	0.933	0.017	0.933	0.933
Damage 5	1.000	0.000	1.000	1.000

5.3. Random forest

The random forest demonstrated even better classification accuracy both in cross-validation and testing (98.67% in both). The cross-validation results are presented in Table 5 and Fig. 16, while the testing results are shown in Table 6 and Fig. 17.

TABLE 5. Class-wise accuracy table.

Class	TP rate	FP rate	Precision	Recall
Healthy	0.980	0.012	0.942	0.980
Damage 1	1.000	0.000	1.000	1.000
Damage 2	1.000	0.000	1.000	1.000
Damage 3	1.000	0.000	1.000	1.000
Damage 4	0.960	0.004	0.980	0.960
Damage 5	0.980	0.000	1.000	0.980

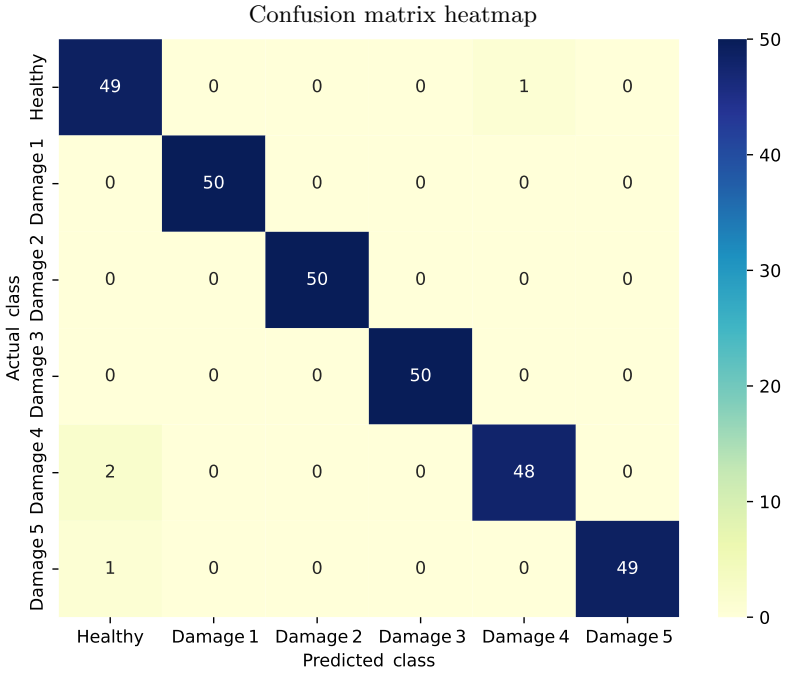

FIG. 16. Cross-validation results for random forest.

Detailed insights are as follows:

- Correctly classified instances: 74/75 (98.67%).
- Kappa statistic: 0.984.
- Weighted average precision: 0.988, recall: 0.987, F-measure: 0.987, and ROC area: 0.996.

TABLE 6. Class-wise accuracy table.

Class	TP rate	FP rate	Precision	Recall
Healthy	1.000	0.016	0.923	1.000
Damage 1	1.000	0.000	1.000	1.000
Damage 2	1.000	0.000	1.000	1.000
Damage 3	1.000	0.000	1.000	1.000
Damage 4	0.933	0.000	1.000	0.933
Damage 5	1.000	0.000	1.000	1.000

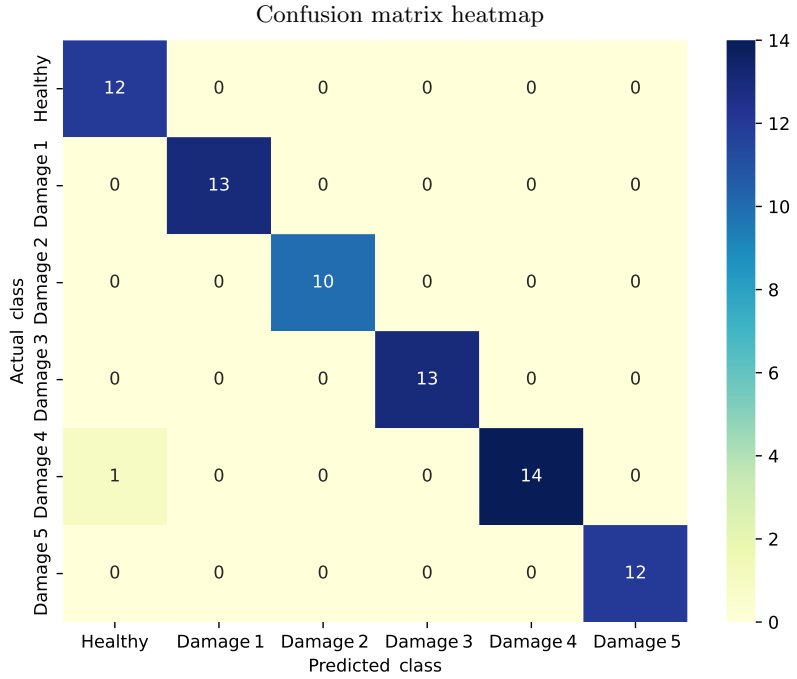

FIG. 17. Test results for random forest.

The confusion matrices (Figs. 16 and 17) show excellent classification performance, with minimal misclassifications occurring between the healthy and damage 1 classes. The remaining damage classes were classified with near-perfect precision and recall, highlighting the robustness of the random forest model.

5.3.1. Key observations

- The performance of the model was consistent between the cross-validation and test datasets, which demonstrates a sufficient level of generalization.

- Features such as `kurtosis`, `zero crossing rate`, and `L2 energy norm` were identified as to be critical for classification process, indicated by the analysis of feature importance scores.
- The reasons for the errors in classification were mostly related to the classes of healthy and damage 5. This outcome is expected as both cases are symmetric with respect to the two actuators. As a result, features based on the difference in time signals from the two actuators were not informative enough, leading to misclassification. Adding more training data related to such symmetric cases could further improve classification performance.

6. Conclusion

The study presents, for the first time, the use of a self-referencing configuration for baseline-free damage localization and should be regarded as a proof-of-concept for this specialized configuration of FBG sensors. The paper, first, employs a traditional ToA technique with a synthesized baseline signal. The ToA based method works in some cases, but gives false detection in others. Also, for the detection more information regarding the velocity of propagation is needed, which makes its application challenging. As a solution, ML-based algorithm was applied to the same dataset. Based on the size of the data, and the availability of labels, the supervised learning approach was used. Since the physics of the coupling mechanism is not yet fully understood, statistical features were used instead. The importance of the different features was identified using different techniques available in the literature. The 10 most important features were then identified and used for classification with three different models. It was noted that random forest is the most appropriate classifier with highest accuracy and generalizability. Feature selection methods highlighted the significance of elements such as `kurtosis`, `zero crossing rate` and `L2 energy norm`, which were among the most important across multiple techniques. Reduction of dimensionality also provided a good understanding into the separability of data, reinforcing the credibility of the chosen features. This study shows that there is a potential for effective ML approach for SHM systems targeted towards effective damage detection. A future work will deal with sophisticated neural network designs as well as deep learning. Furthermore, the proposed methodology will be extended to detect damage at different locations on the plate rather than only on the direct path between the bonds. The authors acknowledge that there is a need for experimental validation, where more uncertainties in the measurements, such as ambient condition changes, deterioration of the sensor bonds, etc., will be captured, and the robustness, sensitivity to damage size and generalizability of the ML-techniques will be benchmarked. In order to show the effectiveness of the method, the ML techniques should be able to identify

damage at unseen locations, or should have in place mechanisms to identify data that is significantly different than the training sets, as suggested in [30]. This indeed is identified as a next step of our research.

Acknowledgments

This research was supported by a project funded by the National Science Center, Poland, titled: Guided waves-based reference-free structural health monitoring using fiber Bragg grating sensors (2020/39/D/ST8/00188). The authors are grateful to TASK-CI for providing access to their computational resources. The opinions expressed in this paper do not necessarily reflect those of the sponsors.

References

1. A. Ghadami, A. Maghsoodi, H. Mirdamadi, A new adaptable multiple-crack detection algorithm in beam-like structures, *Archives of Mechanics*, **65**(6): 469–483, 2013.
2. A. Kakei, J. Epaarachchi, M. Islam, J. Leng, Evaluation of delamination crack tip in woven fibre glass reinforced polymer composite using FBG sensor spectra and thermo-elastic response, *Measurement*, **122**: 178–185, 2018, https://doi.org/10.1016/j.measurement.2018.03.023.
3. S. Sawant, A. Sethi, S. Banerjee, S. Tallur, Unsupervised learning framework for temperature compensated damage identification and localization in ultrasonic guided wave SHM with transfer learning, *Ultrasonics*, **130**: 106931, 2023, https://doi.org/10.1016/j.ultras.2023.106931.
4. B.A. de Castro, F.G. Baptista, F. Ciampa, New signal processing approach for structural health monitoring in noisy environments based on impedance measurements, *Measurement*, **137**: 155–167, 2019, https://doi.org/10.1016/j.measurement.2019.01.054.
5. Q. Bao, T. Xie, W. Hu, K. Tao, Q. Wang, Multi-type damage localization using the scattering coefficient-based RAPID algorithm with damage indexes separation and imaging fusion, *Structural Health Monitoring*, **23**(3): 1592–1605, 2024, https://doi.org/10.1177/14759217231191267.
6. S. Cantero-Chinchilla, J. Chiachío, M. Chiachío, D. Chronopoulos, A. Jones, A robust Bayesian methodology for damage localization in plate-like structures using ultrasonic guided-waves, *Mechanical Systems and Signal Processing*, **122**: 192–205, 2019, https://doi.org/10.1016/j.ymssp.2018.12.021.
7. S. Sampath, H. Sohn, Detection and localization of fatigue crack using nonlinear ultrasonic three-wave mixing technique, *International Journal of Fatigue*, **155**: 106582, 2022, https://doi.org/10.1016/j.ijfatigue.2021.106582.
8. P. Kashyap, K. Shivgan, S. Patil, B.R. Raja, S. Mahajan, S. Banerjee, S. Tallur, Unsupervised deep learning framework for temperature-compensated damage assessment using ultrasonic guided waves on edge device, *Scientific Reports*, **14**(1): 3751, 2024, https://doi.org/10.1038/s41598-024-54418-w.

9. V. Nerlikar, O. Mesnil, R. Miorelli, O. d'Almeida, Damage detection with ultrasonic guided waves using machine learning and aggregated baselines, *Structural Health Monitoring*, **23**(1): 443–462, 2024, https://doi.org/10.1177/14759217231169719.

10. F. Ricci, E. Monaco, N.D. Boffa, L. Maio, V. Memmolo, Guided waves for structural health monitoring in composites: A review and implementation strategies, *Progress in Aerospace Sciences*, **129**: 100790, 2022, https://doi.org/10.1016/j.paerosci.2021.100790.

11. Z. Yang *et al.*, A review on guided-ultrasonic-wave-based structural health monitoring: From fundamental theory to machine learning techniques, *Ultrasonics*, **133**: 107014, 2023, https://doi.org/10.1016/j.ultras.2023.107014.

12. H. Zhu, Z.S. Khodaei, F.M. Aliabadi, Appraisal of linear baseline-free techniques for guided wave based structural health monitoring, *Ultrasonics*, **144**: 107445, 2024, https://doi.org/10.1016/j.ultras.2024.107445.

13. M. Mitra, S. Gopalakrishnan, Guided wave based structural health monitoring: A review, *Smart Materials and Structures*, **25**(5): 053001, 2016, https://doi.org/10.1088/0964-1726/25/5/053001.

14. M. Caponero, Use of FBG sensors in advanced civil engineering applications, *Journal of Instrumentation*, **18**(07): C07020, 2023, https://doi.org/10.1088/1748-0221/18/07/C07020.

15. B. Wang, W. Sun, H. Wang, Y. Wan, T. Xu, Location determination of impact on the wind turbine blade surface based on the FBG and the time difference, *Sensors*, **21**(1): 232, 2021, https://doi.org/10.3390/s21010232.

16. M. Mieloszyk, K. Majewska, W. Ostachowicz, Application of embedded fibre Bragg grating sensors for structural health monitoring of complex composite structures for marine applications, *Marine Structures*, **76**: 102903, 2021, https://doi.org/10.1016/j.marstruc.2020.102903.

17. T. Juwet, G. Luyckx, A. Lamberti, F. Creemers, E. Voet, J. Missinne, Monitoring of composite structures for re-usable space applications using FBGs: The influence of low Earth orbit conditions, *Sensors*, **24**(1): 306, 2024, https://doi.org/10.3390/s24010306.

18. J. Wee, J.M. Kim, K. Peters, Acoustic-optical interactions in optical fiber sensors for ultrasonic inspection of structures, [in:] *OSA Optical Sensors and Sensing Congress 2021*, S. Buckley *et al.* [Eds.], paper STu2B.1, OSA Technical Digest, Optica Publishing Group, 2021.

19. C.S. Marashi, P. Bradford, K. Peters, Laser Doppler vibrometry measurements of acoustic attenuation in optical fiber waveguides, *Applied Optics*, **62**(16): E119–E124, 2023, https://doi.org/10.1364/AO.483827.

20. F. Yu, O. Saito, Y. Okabe, An ultrasonic visualization system using a fiber-optic Bragg grating sensor and its application to damage detection at a temperature of 1000°C, *Mechanical Systems and Signal Processing*, **147**: 107140, 2021, https://doi.org/10.1016/j.ymssp.2020.107140.

21. R. Soman, J.M. Kim, S. Aiton, K. Peters, Guided waves based damage localization using acoustically coupled optical fibers and a single fiber Bragg grating sensor, *Measurement*, **203**: 111985, 2022, https://doi.org/10.1016/j.measurement.2022.111985.

22. J. Wee, K. Alexander, K. Peters, Self-referencing ultrasound detection of fiber Bragg grating sensor remotely bonded at two locations, [in:] *Sensors and Smart Structures Technologies for Civil, Mechanical, and Aerospace Systems 2020*, Vol. 11379, pp. 190–195, SPIE, 2020, https://doi.org/10.1117/12.2559252.

23. J. Wee, K. Alexander, K. Peters, Self-referencing ultrasound detection of fiber Bragg grating sensor with two adhesive bonds, *Measurement Science and Technology*, **32**(10): 105115, 2021, https://doi.org/10.1088/1361-6501/ac065c.

24. P. Fiborek, R. Soman, P. Kudela, W. Ostachowicz, Spectral element modeling of ultrasonic guided wave propagation in optical fibers, *Ultrasonics*, **124**: 106746, 2022, https://doi.org/10.1016/j.ultras.2022.106746.

25. J. Wee, D. Hackney, P. Bradford, K. Peters, Simulating increased lamb wave detection sensitivity of surface bonded fiber Bragg grating, *Smart Materials and Structures*, **26**(4): 045034, 2017, https://doi.org/10.1088/1361-665X/aa646b.

26. M. Goubeaud, P. Joußen, N. Gmyrek, F. Ghorban, A. Kummert, White noise windows: Data augmentation for time series, [in:] *2021 7th International Conference on Optimization and Applications (ICOA)*, pp. 1–5, IEEE, 2021.

27. H. Chen, K. Xu, Z. Liu, D. Ta, Ellipse of uncertainty based algorithm for quantitative evaluation of defect localization using Lamb waves, *Ultrasonics*, **125**: 106802, 2022, https://doi.org/10.1016/j.ultras.2022.106802.

28. Z. Zhang, H. Pan, X. Wang, Z. Lin, Machine learning-enriched lamb wave approaches for automated damage detection, *Sensors*, **20**(6): 1790, 2020, https://doi.org/10.3390/s20061790.

29. G. Park, H.H. Cudney, D.J. Inman, Impedance-based health monitoring of civil structural components, *Journal of Infrastructure Systems*, **6**(4): 153–160, 2000, https://doi.org/10.1061/(ASCE)1076-0342(2000)6:4(153).

30. A. Sanju, A.D. Patange, A.M. Rahalkar, R. Soman, Notifying type-2 error and segregating undefined conditions in health monitoring of milling cutter: A statistical and deep learning approach, *Journal of Vibration Engineering & Technologies*, **13**(1): 1–18, 2025, https://doi.org/10.1007/s42417-024-01706-4.

Received January 15, 2025; revised version May 16, 2025;
accepted June 9, 2025; published online June 18, 2025.